Probing the role of beam remnant diquark fragmentation in particle production in central ^{7}Be + ^{9}Be collisions at energies available at the CERN Super Proton Synchrotron using the improved HIJING code

Khaled Abdel-Waged ⬤* and Nuha Felemban ⬤

Physics Department, Faculty of Applied Science, Umm Al-Qura University, Makkah 21421, Saudi Arabia

The impact of different diquark fragmentation mechanisms on proton, $\pi^{\pm}$, and $K^{\pm}$ spectra in 20% central ^{7}Be + ^{9}Be collisions has been investigated at the CERN Super Proton Synchrotron (SPS) energies using the Heavy Ion Jet Interaction Generator (HIJING) code. The advanced popcorn (AP) string model of PYTHIA 6.4 was employed, and two popcorn scenarios for diquark fragmentation were considered: The simple diquark model and the AP model. The AP mechanism allows for the implementation of beam remnant diquark fragmentation (BRDF), which occurs when a quark is expelled from a proton beam. The AP model provides two possible channels for baryon production from BRDF: The baryon-antibaryon ($B\bar{B}$) configuration, as well as configurations such as $BM\bar{B}$ and $BMM\bar{B}$. In the diquark model, a $B\bar{B}$ is always produced from the diquark-antidiquark ($qq - \bar{q}\bar{q}$) pair production between the original ($q_0 - \bar{q}_0$) jet pair. It is shown that the diquark model is more suitable for explaining the proton density at midrapidity compared to the default AP approach, which exhibits an unusual arrangement of peaks and dips in proton spectra at midrapidity. However, the HIJING/diquark calculations are not consistent with proton diffraction peaks and the production of new particles. On the other hand, the BRDF effects implemented in HIJING/AP are found to be more suited for the description of proton stopping observables in central Be + Be collisions, while still producing the correct $\pi^{\pm}$ and $K^{\pm}$ dN/dy and p_T spectra at midrapidity for the entire range of SPS energies.

I. INTRODUCTION

The NA61/SHINE experiment, conducted at the Super Proton Synchrotron (SPS) facility at CERN, investigates the production of particles resulting from the collision of nuclei of different sizes, over a range of energies spanning from 19A to 150A GeV/c [1,2]. Comparing microscopic transport models of multiparticle production to the SPS regime, where the perturbative sector of quantum chromodynamics (QCD) is inapplicable, poses a significant challenge for current event generators.

The rapidity density (dN/dy) of charged particles, together with their transverse momentum (p_T) spectra and midrapidity values, are fundamental quantities in understanding the underlying mechanisms of hadron production in soft multiparticle processes. Therefore, achieving an accurate description of these parameters is a crucial task in the investigation of proton-proton (pp) and nucleus-nucleus (AA) collisions at the SPS regime. In the context of inelastic nucleon-nucleon (NN) collisions, "soft" refers to processes where the transverse momenta of the produced particles are on the order of a few GeV/c. At the SPS energy range, such processes dominate the inelastic NN cross section and are typically modeled using string-based approaches [3–11].

Recently, new data have been acquired concerning the inclusive charged particle distributions that arise from collisions between the lowest mass isospin symmetric systems, such as the Be + Be collisions at SPS energies [2]. These measurements could lead to a better theoretical understanding of baryon stopping in heavy-ion collisions at CERN SPS energies, particularly since protons are a fairly abundant product of nuclear collisions within this energy range.

In collisions that involve lighter systems such as Be + Be, the proton rapidity spectra exhibit a dip at midrapidity ($y \approx 0$) across all beam energies [2]. However, the Heavy Ion Jet Interaction Generator (HIJING) [3] suggests that the proton distribution at midrapidity in these reactions shifts from a convex shape (reflecting strong stopping) to a concave shape (indicating increasing transparency) as the beam energy increases, as illustrated in Fig. 6 of Ref. [12]. A recent comparison between string-based models (e.g., [4,5,13,14]) and the measured dN/dy and p_T spectra from NA61/SHINE data revealed significant discrepancies at various SPS energies. Figures 31, 34, and 35 of Ref. [2] illustrate these differences. The comparison demonstrated that ultrarelativistic quantum molecular dynamics (UrQMD) (version 3.04) [5] and a multiphase transport (AMPT) (1.26) [4] models overestimate the dN/dy and p_T spectra of protons, π^-, and $K^{\pm}$ in central Be + Be collisions at 40A and 150A GeV/c. Furthermore, Ref. [2] also pointed out that the Parton-Hadron-String Dynamics model [13], which incorporates partonic interactions in-and-out of equilibrium, the Lund string model of PYTHIA6.4

[15], and final scattering of hadrons, failed to accurately describe the rapidity and p_T spectra of identified hadrons at midrapidity ($0 < y < 0.2$). Consequently, constructing a dependable phenomenological model that describes the spectra of emitted protons at SPS energies still remains a significant challenge that requires extensive theoretical efforts.

In this work, the production of identified hadrons in 20% central Be + Be collisions has been investigated at various SPS energies [2]. To achieve this, HIJING 1.383 [3] is utilized in conjunction with the advanced popcorn (AP) baryon production mechanism [11], which is incorporated into the PYTHIA6.4 event generator [15]. Additionally, an extensive comparison is conducted of the results obtained from HIJING, utilizing two different diquark fragmentation scenarios of the popcorn mechanisms of baryon production: The diquark model [9] and the beam remnant diquark fragmentation (BRDF) model [11]. The diquark model produces a baryon-antibaryon ($B\bar{B}$) pair from the diquark-antidiquark ($qq - \bar{q}\bar{q}$) pair production between the original ($q_0 - \bar{q}_0$) jet pair [9]. On the other hand, the AP mechanism incorporates the BRDF, which is generated when a quark is expelled from a proton beam [11]. The BRDF is treated as a single entity and fragments directly into a $B\bar{B}$ channel. Additionally, the BRDF breaking component allows for cases where only one of the two quarks enters the produced baryon, while the other remains in the meson ($BM\bar{B}$ channel). As will be discussed below, a critical component required for describing soft NN processes at SPS energies is the implementation of the BRDF component into the Lund model to achieve a more precise representation of baryon stopping in central Be + Be collisions.

The structure of the paper is as follows. In Sec. II, an overview is provided of the essential components of the HIJING model coupled with diquark and AP/BRDF models. In Sec. III, the results of our analysis are presented, where the models are compared to experimental data from the NA61/SHINE [1] for proton, $\pi^{\pm}$, and $K^{\pm}$ spectra in 20% central Be + Be collisions at four different beam momenta (30, 40, 75, and 150 AGeV/c). Finally, in Sec. IV, our findings are summarized and conclusions are drawn.

II. DESCRIPTION OF THE MODEL

This section provides a brief overview of the HIJING model [3], which is combined with the diquark and advanced popcorn (AP) mechanisms of baryon production [11]. A comprehensive explanation of this model can be found in Refs. [3,11,16–18].

The HIJING model is built upon the *pp*-dynamics extrapolation and employs the Glauber calculation to determine the number of inelastic nucleon-nucleon (NN) collisions [3]. These collisions are classified into two types: Soft NN collisions treated according to the FRITIOF model, and hard parton-parton collisions treated as in PYTHIA. The multiple string phenomenology, which is based on the creation of excited color singlet states known as "strings," is used to describe soft primary collisions with multiparticle production at intermediate CERN SPS energies. This phenomenology has been developed in Refs. [6,7,19,20] for energetic hadron-hadron (hh) collisions. On the other hand, hard collisions are

characterized by the inclusive jet cross section (σ_{jet}) of minijet production, and they are included using standard perturbative QCD (pQCD) for events with large transverse momentum ($p_T \geqslant 2$ GeV/c) [3].

The HIJING/AP code [3,11] incorporates three different processes for the excitation of a soft string: (i) single diffractive, (ii) double diffractive, and (iii) nondiffractive. In this work, all soft string processes utilize the Lund model of PYTHIA6.4 [15] for string decay into final state hadrons. It is important to note that the HIJING/AP version of PYTHIA 6.4 includes not only the AP [11] mechanism for baryon production, but also the diquark [9] and simple popcorn [10] mechanisms, which distinguishes it from the default HIJING that utilizes JETSET/PYTHIA 5.2 [8,21,22].

The Lund string model [6–8] describes hadron-hadron collisions as multiple soft gluon exchange between valence quarks or diquarks which leads to the creation of a high tension string (flux tubes stretched between the endpoints), with a string tension $k_0 \simeq 1$ GeV/fm. In the simple diquark model, the breaking of a string can occur via quark-antiquark or antidiquark-diquark pair production [9]. The AP model [11], on the other hand, is a more complex scenario where diquarks do not exist as such, but rather quark-antiquark pairs are produced one after the other. In this study, two cases are considered in the AP model: (i) the endpoint of the original $q_0 - q_0q_0$ string of a proton beam is a leading quark (LQ), and (ii) the generalization to a beam remnant diquark fragmentation (BRDF) jet, which occurs when a quark is kicked out of a proton beam. In the diquark model, the baryon (B) and antibaryon ($\bar{B}$) are always produced as nearest neighbors along the string, whereas in the AP scenario, many mesons may be produced.

The production of mesons with varying flavors and spins is explained as a tunneling phenomenon, which results in the disruption of the string through the creation of a vertex pair consisting of a $q'_1 - \bar{q}1'$ pair from the initial $q_0 - \bar{q}_0$ jet pair. The rate of production for a vertex pair ($q'_i - \bar{q}'_i$) is determined using the Schwinger formula [23]

$$P_{q'-\bar{q}'} \approx \exp\left(-\pi m_{\perp q'}^2/k_0\right). \tag{1}$$

The transverse mass of the pair of quarks, with mass $m_{q'}$ and transverse momentum $p_{\perp}$, is given by $2m_{\perp q'} = 2\sqrt{m_{q'}^2 + p_{\perp}^2}$. If the invariant mass of either of the two color singlet systems $q_0\bar{q}'_1$ and $q'_1\bar{q}_0$ is sufficiently high, further breaks may occur, resulting in the production of n mesons, i.e., $q_0 - \bar{q}'_1$, $q'_1 - \bar{q}'_2, \ldots, q'_{n-1} - \bar{q}_0$. The formula (1) shows a suppression of strange $s - \bar{s}$ pairs in relation to light $q' - \bar{q}'$ pairs with a ratio of $u - \bar{u}: d - \bar{d}: s - \bar{s} = 1:1: \gamma_s = P_{s-\bar{s}}/P_{q'-\bar{q}'}$, where $\gamma_s = 0.3$ is the default value [9,10].

The diquark model proposes that a $B - \bar{B}$ pair can be produced in a manner similar to the production of mesons [9]. Specifically, it suggests that if a diquark-antidiquark pair is produced due to the breaking of a string, which forms a color (anti)triplet, then a $B - \bar{B}$ pair can be created. In this scenario, the $B - \bar{B}$ pair will always have two quark flavors in common and be located near each other in momentum space, see Fig. 1.

The diquark model includes several parameters that relate to tunneling suppressions [9]. These include: (i) the diquark
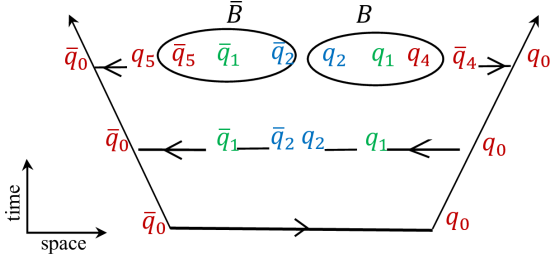
FIG. 1. Illustration depicting the breakup of a diquark $(q_1 q_2)$ in a $B - \bar{B}$ configuration. A color field is stretched between a pair of red-antired $q_0 \bar{q}_0$. If a diquark $q_1 q_2 - \bar{q}_1 \bar{q}_2$ pair (treated as a single entity) is produced within this region, the color field can break and form a $B - \bar{B}$ pair as nearest neighbors.

suppression factor, $\gamma_{qq} = P_{qq-\bar{q}\bar{q}}/P_{q-\bar{q}}$, which is the ratio of production rates of diquark-antidiquark to quark-antiquark pairs; (ii) the strangeness suppression factor, γ_s; (iii) the additional suppression associated with a diquark containing a strange quark compared to the normal suppression of a strange quark, $\gamma_{qs} = (\gamma_{us}/\gamma_{ud})/\gamma_s$; and (iv) the suppression of spin 1 diquarks relative to spin 0 ones, $\gamma_{10} = (1/3)(\gamma_{ud_1}/\gamma_{ud_0})$.

It is important to note that in addition to these factors, the probability of obtaining a particular baryon is influenced by the likelihood of the diquark and quark forming a symmetric three-quark state, which corresponds to all states being in the SU(6) group [15].

The AP model proposes that baryons are formed through the successive creation of multiple $q_i - \bar{q}_i$ pairs, produced from a pair of LQ jets [11], see Fig. 2. It is assumed that a color field extends between the leading q_0 (red r) and $\bar{q}_0$ ($\bar{r}$) pair. Within this field, a $q_1 - \bar{q}_1$ pair can be produced as a fluctuation with $g\bar{g}$ (g = green), which is not sufficient to split the string into two singlet states. Such quarks are referred to as "curtain" pairs. In contrast, the production of a vertex pair
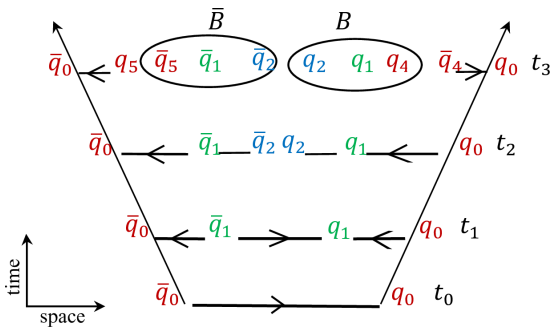

FIG. 2. Illustration showcasing the popcorn breakup of a diquark $(q_1 q_2)$ in a $B - \bar{B}$ configuration. At t_0, a complete string is formed between a red-antired $q_0 \bar{q}_0$ pair. At t_1, a virtual fluctuation leads to the creation of a green-antigreen $q_1 \bar{q}_1$ pair. This causes a change in the color field from red-antired to blue-antiblue, along with a reversal in the field direction (from triplet to antitriplet). At t_2, the string breaks as a result of the production of a blue-antiblue $q_2 \bar{q}_2$ pair, generating two string segments with diquark endpoints. By t_3, two new red-antired ($q_4 \bar{q}_4$ and $q_5 \bar{q}_5$) pairs are formed, leading to the creation of a baryon-antibaryon pair.

$q - \bar{q}$, which breaks the string, is determined by Eq. (1) in the AP model, even when it results in a diquark. The suppression of all vertex quarks, whether they are diquarks or s quarks, is thus determined by the parameters $\gamma_{qq} = P_{qq-\bar{q}\bar{q}}/P_{q-\bar{q}}$ and γ_s.

Since there is no net force acting on the $q_1 - \bar{q}_1$ curtain pair, they are observed as free particles. The probability of producing these quarks at a separation distance of d is determined by [11]

$$P_{q-\bar{q}} \approx \exp\left(-2m_{\perp q}^2/k_0\right), \qquad (2)$$

where $m_{\perp q}$ is the transverse mass of the curtain quark. When the q_0 and q_1 quarks form an antitriplet color state ($r + g = \bar{b}$, where b = blue), the remaining net color field between q_1 and $\bar{q}_1$ corresponds to a triplet color field $b\bar{b}$ of the same strength as the original field. Within the color fluctuation region, an additional curtain $q_2 - \bar{q}_2$ pair can be produced, where q_2 is attracted towards $q_0 q_1$ and $\bar{q}_2$ towards $\bar{q}_0 \bar{q}_1$, with no net color field between q_2 and $\bar{q}_2$. If additional vertices $q_4 - \bar{q}_4$ and $q_5 - \bar{q}_5$ break occur between q_0 and q_1 and $\bar{q}_0$ and $\bar{q}_1$, a baryon (B) is created consisting of $q_1 q_2$ and q_4, while an antibaryon ($\bar{B}$) is formed consisting of $\bar{q}_1 \bar{q}_2$ and $\bar{q}_5$, see Fig. 2. These baryon and antibaryon configurations are nearest neighbors in rank and share two quark pairs, i.e., $q_1 q_2 q_4 - \bar{q}_1 \bar{q}_2 \bar{q}_5$ in a $B\bar{B}$ configuration, see Fig. 2.

The probability of baryon formation in the $B\bar{B}$ configuration scheme resulting from LQ jet production is calculated using [11]

$$P_B \approx \exp(-4\mu_\perp^2/k_0), \qquad (3)$$

where $\mu_\perp = m_{\perp q_1} + m_{\perp q_2}$ is the transverse mass of diquark. The term $\mu_\perp/k_0$ represents the distance that the effective $q_1 q_2$ diquarks must tunnel through to reach the mass shell. This implies that larger diquark masses are suppressed as if they had tunneled as a single unit. It is important to note that the probability of obtaining a certain baryon is weighted by the probability that the diquark and the quark form symmetric three-quark states, which means that all states must adhere to the SU(6) symmetry [11].

In the case where a meson system $q_2 \bar{q}_3$ is produced with an invariant mass of $M_\perp$ between a baryon $q_1 q_3 q_4$ and an antibaryon $\bar{q}_1 \bar{q}_2 \bar{q}_5$, a $BM\bar{B}$ configuration is formed, see Fig. 3. It should be noted that, unlike the $B\bar{B}$ configuration, the B and $\bar{B}$ in $BM\bar{B}$ share only one quark-antiquark pair. For the $BM\bar{B}$ configuration, the q_1 and $\bar{q}_1$ must tunnel an additional distance $d = (M_\perp + m_{\perp q_2} + m_{\perp q_4})/k_0$ in order to create space for the meson to be formed from the energy density in the middle. Therefore, the suppression of popcorn mesons in the $BM\bar{B}$ configuration scheme from LQ jet is given by [11]

$$P_{LQ} \approx \exp(-2m_{\perp q}d), \qquad (4)$$

where $m_{\perp q}$ is the transverse mass of the curtain quark. The $B\bar{B}$ configuration channel in Eq. (3) is very similar to the configuration channel at a distance $d = 2m_{\perp q}/k_0$. Hence, the production of baryons by LQ jet is governed by the $B\bar{B}$ and $BM\bar{B}$ channels, as given by Eq. (4). The relative production rates for different diquark masses, the type of curtain quark (light or strange), and the mass of the leading rank meson determine these channels. In the AP model, the average
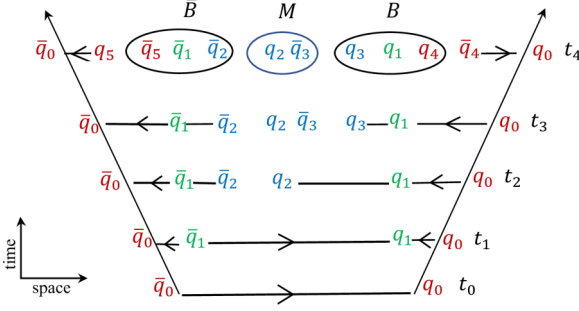
FIG. 3. Illustration depicting the popcorn breakup of a diquark $(q_1 q_2)$ in a $BM\bar{B}$ configuration. At t_0, no fluctuations have occurred, and a complete string connects a red-antired $q_0 \bar{q}_0$ pair. At t_1, a quantum fluctuation leads to the emergence of a green-antigreen $q_1 \bar{q}_1$ pair on the string. If the red and green quarks form an antiblue triplet, it reverses the color flow in that segment of the string, resulting in zero net force acting on the green quark. At t_2, the string breaks due to the production of a blue-antiblue $q_2 \bar{q}_2$ pair, leading to the formation of two string segments with diquark endpoints. At t_3, another breakup occurs within the blue triplet field, resulting in an additional blue-antiblue $q_3 \bar{q}_3$ pair. By t_4, two new red-antired ($q_4 \bar{q}_4$ and $q_5 \bar{q}_5$) pairs have been generated. The outcome is a baryon-antibaryon pair with a meson in between.

transverse momentum $< m_{\perp q_1} >$ for light (u) and strange (s) quarks is determined by two parameters [11]

$$\beta_u = 2 < m_{\perp u} > /k_0 \quad \text{and} \quad \Delta\beta = \beta_s - \beta_u, \tag{5}$$

which determines the relative rates of different diquark production and the production of intermediate popcorn mesons in the $BM\bar{B}$ configuration channel. The AP model [11] also considers configurations such as $BMM\bar{B}$ and $BMMM\bar{B}$.

Thus, the AP mechanism implements two processes for baryon production: (i) the two quarks of the effective diquark enter the same leading baryon $q_1 q_2 \rightarrow (q_1 q_2 q_4)B + \bar{q}_4$, and (ii) a meson is first produced, containing one of the quarks, while the other is contained in the baryon in the next step, $q_1 q_2 \rightarrow (q_2 \bar{q}_3)M + (q_1 q_3 q_4)B + \bar{q}_4$. Furthermore, since the three quarks of the produced baryon are mostly independent, the model takes into account a suppression of higher spin states. Specifically, there is a suppression of ud quark pairs compared to us or ds pairs, as larger spin-spin interactions are present [11].

In certain cases, the endpoint of a string is not a single quark but rather a diquark, typically observed when a quark is expelled from a proton beam particle. To account for baryon production in a $q_0 - \bar{q}_0$ string, an algorithm can be applied to the fragmentation of a string initially containing a diquark. In this scenario, the string with a diquark endpoint is assumed to behave similarly to the remaining portion of a $q_0 - \bar{q}_0$ string, as depicted in Fig. 4. Thus, a $q_0 q_0$ diquark endpoint is treated as having the flavor $q_1 q_2$. This means that either the two quarks of the $q_0 q_0$ diquark enter the same leading baryon, or a meson is first produced containing one of the quarks, while the other is subsequently incorporated into the baryon. In such cases, the fragmentation of the resulting beam remnant diquark (BRDF) is subject to exponential suppression, similar to the advanced popcorn mechanism. However, due to the
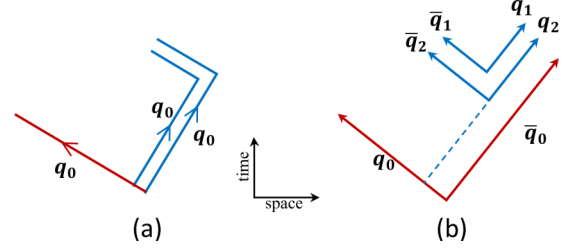

FIG. 4. (a) String breakup in a leading diquark jet. (b) String breakup in a leading quark jet.

BRDF's significant contribution to the momentum of the incoming proton and its faster average behavior, the production of baryons from the LQ jet in Eq. (4) is expected to vary across different beam energies. Consequently, the production of baryons from the BRDF is controlled by

$$P_{\text{BRDF}} \approx \exp(-\beta' d). \tag{6}$$

Therefore, the strength of the baryon production mechanism in the BRDF scenario can be described by an equation similar to the one employed for the LQ jet, i.e., Eq. (4), but with a parameter denoted by β' that accounts for the suppression of the diquark jet. To quantitatively evaluate this mechanism, the HIJING framework has been enhanced, and it has been demonstrated that proton stopping in inelastic pp collisions can be accurately predicted by the AP model over a specific range of center-of-mass energy ($6.3 \leqslant \sqrt{s_{\text{NN}}} \leqslant 17.3$ GeV) if β' increases with the energy as

$$\beta'(s) = 4.5 \left(\frac{s}{s_0}\right)^{-0.8}. \tag{7}$$

The scale factor $\sqrt{s_0} = 6.0$ GeV is introduced to adjust the threshold value of the string routines in HIJING, allowing for greater flexibility. By default, the string routines in HIJING are applicable for $\sqrt{s_0} = 10$ GeV. The aforementioned equation results in a significant reduction of diquark and leading rank meson production in the $B\bar{B}$, $BM\bar{B}$, and $B \ldots MM \ldots \bar{B}$ channels. The diquark suppression parameter β' becomes stronger as the beam energy decreases, with β' increasing from ≈ 1 at $\sqrt{s_{NN}} = 17.3$ GeV to 4.5 at $\sqrt{s_{NN}} = 6.3$ GeV.

Furthermore, in AA collisions, the impact of BRDF jet could potentially increase due to in-medium effects or dependence on the number of participants. This increase is accounted for in our analysis by incorporating a power-law dependence, denoted as $\beta' = \beta'(s, A)$,

$$\beta'(s, A) = \beta'(s)A^{1/3} = 4.5 \left(\frac{s}{s_0}\right)^{-0.8} A^{1/3}. \tag{8}$$

The application of Eq. (8) results in β' values of 9.0 and 1.7 for 20% central Be + Be collisions with beam momenta of $19A$ and $150A$ GeV/c, respectively.

Hence, the baryon multiplicities in the AP model are influenced by two parameters, namely, β_u and $\Delta\beta$, in addition to the meson rates-determined parameter γ_s and the diquark probability parameter γ_{qq}. Therefore, a total of four parameters govern the baryon multiplicities. These parameters are implemented in PYTHIA 6.4 routines [15] and are denoted as

TABLE I. Parameter configurations employed in HIJING combined with the simple diquark (DQ) and advanced popcorn (AP) mechanisms for inelastic $p + p$ and central Be+Be collisions at SPS energies. For the HIJING/AP model, the parameters left blank are adopted from the AP mode.

	HIJING/diquark					
Mode	γ_{qq}	γ_s	γ_{qs}	γ_{10}	a	b GeV^{-2}
DQ	0.12	0.22	0.4	0.05	0.5	0.9

	HIJING/advanced popcorn						
Mode	γ_{qq}	γ_s	β_u GeV^{-1}	$\Delta\beta$ GeV^{-1}	β'	a	b GeV^{-2}
AP	0.12	0.22	1.0	1.2	1.0	0.5	0.9
BRDF/pp	–	–	–	–	$\beta'(s)$	–	–
BRDF/AA	–	–	–	–	$\beta'(s, A)$	–	–

follows: $\gamma_{qq} = \text{PARJ}(1)$, $\gamma_s = \text{PARJ}(2)$, $\beta_u = \text{PARJ}(8)$, and $\Delta\beta = \text{PARJ}(9)$.

The AP model assumes that each vertex pair $q' - \bar{q}'$ created through the tunneling mechanism is given a transverse momentum p_T, characterized by a Gaussian width $\sigma_{q'}$ that is shared between the q' and $\bar{q}'$ members of the pair. The transverse momentum of a hadron is obtained as the vector sum of the q' and $\bar{q}'$ kicks, resulting in $\langle p_{T\text{had}}^2 \rangle = 2\sigma_{q'}^2$. In PYTHIA 6.4 program, this process is governed by a single parameter $\sigma_{q'} = \text{PARJ}(21) = 0.36\,\text{GeV}/c$, where a diquark is treated as a single quark [15].

The determination of longitudinal momentum (p_z) of a hadron is based on the requirement that the fragmentation process should look identical regardless of whether the iterative process starts from the q' or the $\bar{q}'$ end. This constraint is achieved by using the Lund symmetric fragmentation function [24],

$$f(z) \propto \frac{1}{z}(1 - z)^a \exp\left(-\frac{bm_{\perp\text{had}}^2}{z}\right), \qquad (9)$$

where a and b are free parameters of the model. The momentum of a hadron i is limited by its transverse mass $m_{\perp\text{had}}$, which implies that $(E_i + p_{zi})(E_i - p_{zi}) = m_{\perp\text{had}}^2$. Therefore, the variable z is determined as the fraction of $(E_i + p_{zi})$ that is taken by the hadron out of the available $\sum_i E_i + p_{zi}$.

In the following discussion, HIJING calculations utilizing the diquark and advanced popcorn mechanisms are referred to as HIJING/diquark and HIJING/AP, respectively. To investigate the impact of baryon production mechanisms on identified hadron species in SPS data, the HIJING/diquark(AP) is employed, and the parameter sets outlined in Table I are considered.

In numerical computations, the HIJING code operates in four different modes: (i) the simple diquark (DQ) mode, where $B - \bar{B}$ pairs are produced from diquark-antidiquark pair production between the initial $q_0 - \bar{q}_0$ jet pair; (ii) the default AP mode, which utilizes the value $\beta' = \beta u = 1$ to simulate baryon production; (iii) the BRDF mode with $\beta' > \beta_u$, where diquark suppression becomes stronger as the collision energy

decreases in accordance with Eq. (7); and (iv) the same as (iii), but with medium effects taken into account as detailed in Eq. (8). In the subsequent analysis, the HIJING/BRDF calculations based on modes (iii) and (iv) are referred to as BRDF/pp and BRDF/AA, respectively. In both modes, the advanced popcorn mechanism is employed for baryon production.

For the calculations of rapidity and transverse momentum spectra of identified hadrons in inelastic pp and central Be + Be collisions, theoretical results obtained from pp collisions at the highest SPS energy of 158 GeV/c, using the parameter set listed in Table I, are used as the baseline for our calculations. The purpose of the tuning process is to ensure that the modified model has a global data description that is at least as good as the previous version of the model [16]. However, to limit the scope of the process, only parameters directly affected by the changes are retuned, and default values are used for other parameters related to fragmentation and tunneling suppressions. The set of resulting parameters should not be considered a new full tune, but rather a confirmation that the added model enhances the overall description while providing a reasonable set of parameters [16]. Depending on the selected parameter set, the HIJING/diquark and HIJING/AP outcomes in 0%–20% central Be + Be collisions at CERN SPS energies can therefore be considered as actual predictions.

Table I employs the default values of a and b parameters of the z longitudinal fragmentation function from HIJING [3]. The values of the diquark ($\gamma_{q'q'}$) and strangeness (γ_s) suppression factors are determined by $\bar{p}$ and K^+ production, respectively. It is important to note that $\Delta\beta$ and β' are the default PYTHIA6.4 parameters for the AP mechanism [11]. To maintain an average of one-half primary mesons produced between B and $\bar{B}$ by the diquark and AP mechanisms [11], the β_u parameter of AP is modified from $\beta_u = 0.6$ to $\beta_u = 1$.

III. RESULTS AND DISCUSSION

In this section, the HIJING model's predictions for different baryon production mechanisms will be applied to investigate 20% central Be + Be collisions at CERN SPS energies, using the parameters listed in Table I. The recent NA61/SHINE measurements of proton, $\pi^{\pm}$, and $K^{\pm}$'s rapidity distributions (dN/dy) and transverse momentum (p_T) spectra will also be compared with these mechanisms. To account for the measurement of rapidities in minimum bias, 10^5 events will be generated for the 0%–20% centrality bin, and the Glauber model's forward energy selection (E_f) provided in Table 2 of Ref. [2] for this bin will be applied. The analysis of the transverse momentum spectra will be limited to the measured rapidity range of $0 < y < 0.2$ in this case.

In Fig. 5, the energy-dependent multiplicity density of midrapidity p, π^+, and K^+ in inelastic pp collisions at SPS energies is shown. These results are obtained from the HIJING model using the diquark and AP mechanisms of baryon production. The results obtained from the HIJING model using the diquark and AP mechanisms of baryon production are compared with the corresponding data from the NA61/SHINE experiment. The two models differ in their treatment of baryon production, where one model involves the production of baryons from diquark-antidiquark ($qq - \bar{q}\bar{q}$) pairs, and the

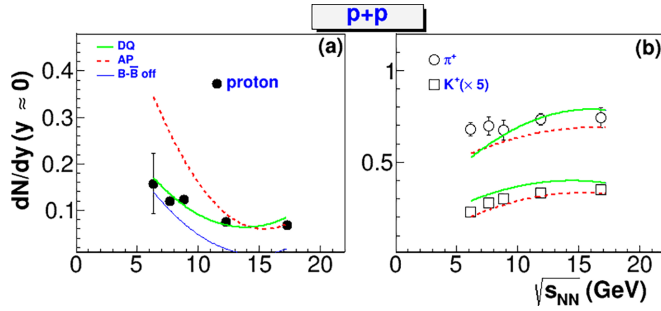FIG. 5. The multiplicity density of protons, π^+ and K^+ at midrapidity ($y \approx 0$) in inelastic pp collisions at the whole SPS energies. The thick and short-dashed lines represent HIJING calculations with diquark and AP models, respectively, while the thin line denotes HIJING calculations without any popcorn mechanism. The closed and open points represent NA61/SHINE data [1].

FIG. 6. Same as Fig. 5, but here the solid and short-dashed lines represent HIJING calculations with AP and AP/BRDF models, respectively.

other model involves the successive production of quark-antiquark ($q - \bar{q}$) pairs. For the purpose of comparison, the results obtained from HIJING without the baryon-antibaryon ($B - \bar{B}$) production mechanism are included (represented by thin lines).

In this case, the diquark at the end of the proton beam is treated as a single entity and directly fragments into a leading baryon. To disable the $B - \bar{B}$ pairs in HIJING and PYTHIA6.4 settings, the main switches IHPR2(11) = 0 and MSTJ(12) = 0 are respectively used.

As illustrated in Fig. 5(a), the proton density at $y \approx 0$ decreases quite rapidly with energy in the absence of the $B - \bar{B}$ channel of the diquark model, which is in disagreement with the measured data. However, this channel fills in the dramatic decrease present in the latter case for $\sqrt{s_{NN}} >$ 6.3 GeV and agrees better with the measured data. Therefore, the diquark model is more effective in describing the proton density at midrapidity than the default AP approach, which treats baryon production from successive production of several $q_i' - \bar{q}_i'$ pairs.

Figure 5(b) display the multiplicity density of π^+ and K^+ at $y \approx 0$ as a function of beam energy. Both calculations with and without the diquark model of $B - \bar{B}$ pair production match well with the experimental data, as shown in the figure. This is expected since both mechanisms assume string breaking of the leading quark end of the proton beam by the production of a vertex $q - \bar{q}$ meson between the original $q_0 - \bar{q}_0$ jet pair. However, it is also evident that the results depend on the $B \ldots MM \ldots \bar{B}$ channel implemented in the AP mechanisms. This implies that the identified mesons are sensitive to the baryon production mechanisms employed in HIJING.

In order to examine the impact of beam remnant diquark fragmentation (BRDF) on the particle density at $y \approx 0$ in inelastic pp collisions at SPS energies, the measured data are compared to both HIJING/AP with and without BRDF in Fig. 6. At $\sqrt{s_{NN}} <$ 17.3 GeV, it is observed that including BRDF into HIJING/AP leads to a closer agreement with the experimental data. Particularly, it is noticed that the proton density at low SPS energies is significantly reduced when
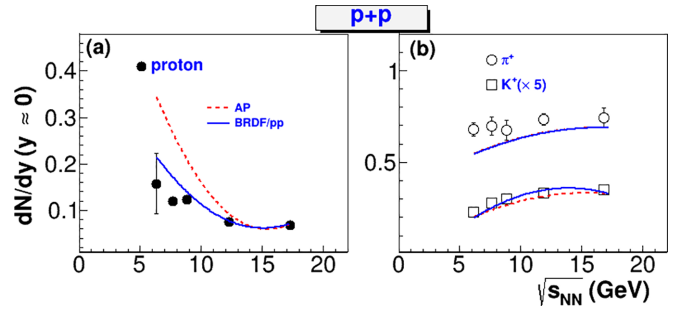
BRDF with $\beta' > \beta_u$ is incorporated in HIJING/AP. Additionally, the multiplicity density of strange K^+ particles slightly increases. This suggests that the BRDF effect in HIJING/AP has a noteworthy role in proton stopping in inelastic pp collisions at CERN SPS energies.

In Fig. 7, the results of HIJING/diquark and HIJING/AP for the proton rapidity distributions (dN/dy) in inelastic pp and 20% central Be + Be collisions are compared with the corresponding experimental data. The HIJING code allows for the exploration of differences between baryon production mechanisms within the framework of PYTHIA6.4 code. It is observed that variations in proton stopping in pp and Be + Be collisions at SPS energies are caused by different realizations of the diquark and popcorn mechanisms.

Specifically, the proton rapidity spectra show a dip at midrapidity for all energies in the case of pp collisions. However, in central Be + Be collisions, a noticeable transition from peak [Fig. 7(a)] to dip [Fig. 7(e)] shapes is visible in AP calculations, which is not present in the experimental data. This behavior suggests a possible influence of the $BM\bar{B}$ channel in the AP mechanism. In contrast, the diquark mechanism predicts no peak-dip transitions for the studied reactions, in agreement with the measured data.

The impact of BRDF on the proton rapidity spectra at various SPS energies is examined by comparing the results of /AP with those of /BRDF, both with and without medium effects, as illustrated in Figs. 7 and 8. It is interesting to note that the "peak-dip" anomaly is entirely absent with BRDF. As shown in Fig. 7, the BRDF calculations effectively capture the midrapidity region of proton rapidities for the studied reactions at SPS energies. In the case of 20% central Be + Be collisions, differences in the midrapidity region arising from medium effects become more prominent as the beam energy decreases. This behavior is linked to the enhancement of suppression of BRDF component with decreasing collision energy.

Figures 7 and 8 illustrate that the inclusion of the BRDF component in central Be + Be collisions, with a relative size determined from pp collisions as described in Sec. II, leads to a proton rapidity distribution that is in agreement with experimental observations at midrapidity. Additionally, it is observed that the different treatments of baryon production mechanisms have a notable impact on the diffraction peaks of
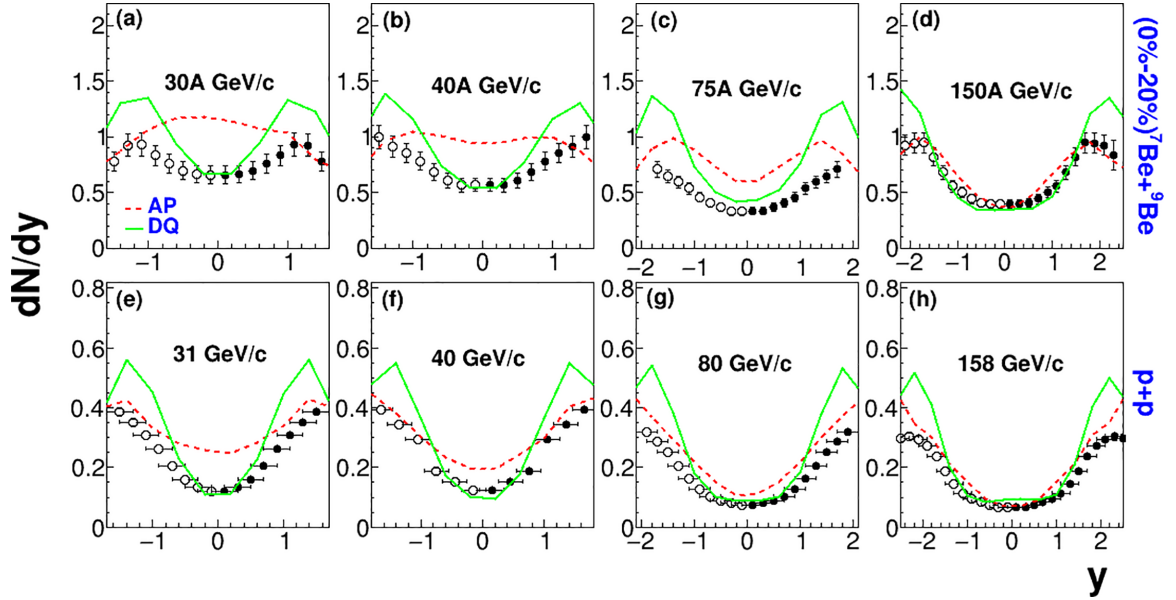
FIG. 7. Rapidity distributions of protons in inelastic *pp* (lower panels) and 20% central Be + Be (upper panels) collisions at different SPS energies. HIJING/diquark and HIJING/AP calculations are shown by the solid and small-dashed lines, respectively. The experimental data (closed points) are from NA61/SHINE measurements [1,2].

the proton, which are located at the projectile beam rapidity ($y = y_{beam}$), as seen in the upper panel of Fig. 8.

Specifically, the diquark mechanism in HIJING overestimates the height of the diffractive peak considerably in contrast to experimental measurements with an increase in beam energy. Conversely, the incorporation of BRDF effects accurately represents diffractive peaks at the highest SPS energy. The favorable agreement of AP/BRDF with the data obtained from NA61/SHINE at forward rapidity signifies the influence of baryon production through sequential $q - \bar{q}$

formations, as opposed to $qq - \bar{q}\bar{q}$ pairs in the diquark model. In this case, at very forward rapidity ($y \approx y_{beam}$), protons are suppressed due to $BM\bar{B}$ channel, resulting in a slower final state proton, as shown in Fig. 8(d).

Thus, the diquark model and BRDF effects have provided a comprehensive understanding of proton production at midrapidity. As collision energy decreases, a significant number of protons are displaced from central to forward rapidity, as evidenced by Figs. 7 and 8. The resulting effects on the dynamics of the newly produced particles are analyzed in Figs. 9 and 10.
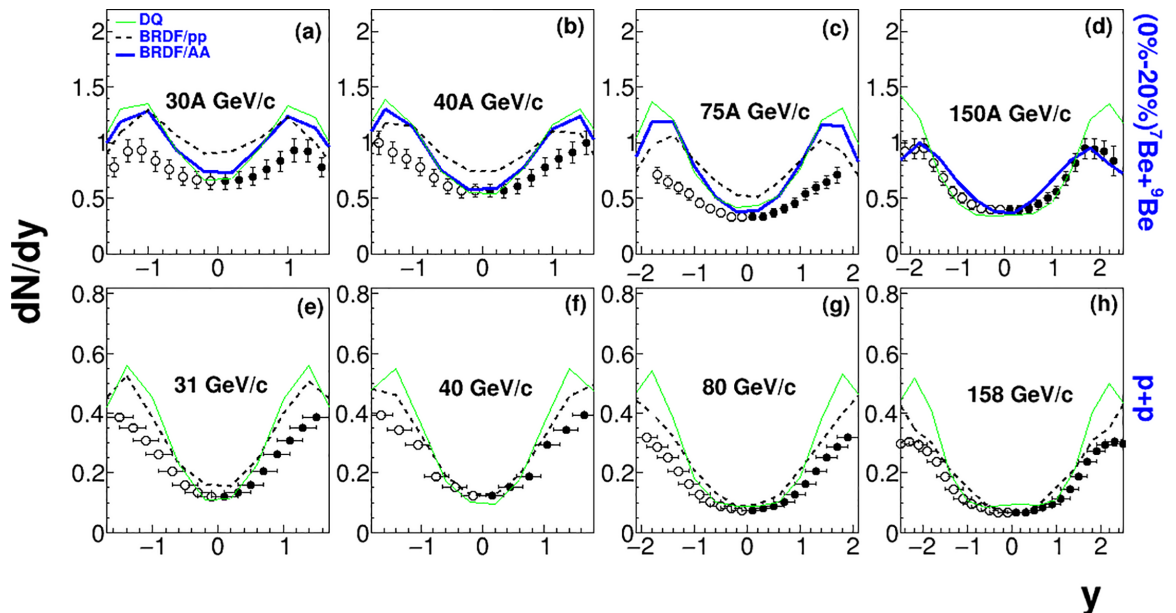

FIG. 8. Same as in Fig. 7, but here the thin solid lines denote HIJING/diquark calculations, while the thick and short-dashed lines represent HIJING calculations using the BRDF mechanism with and without medium effects.
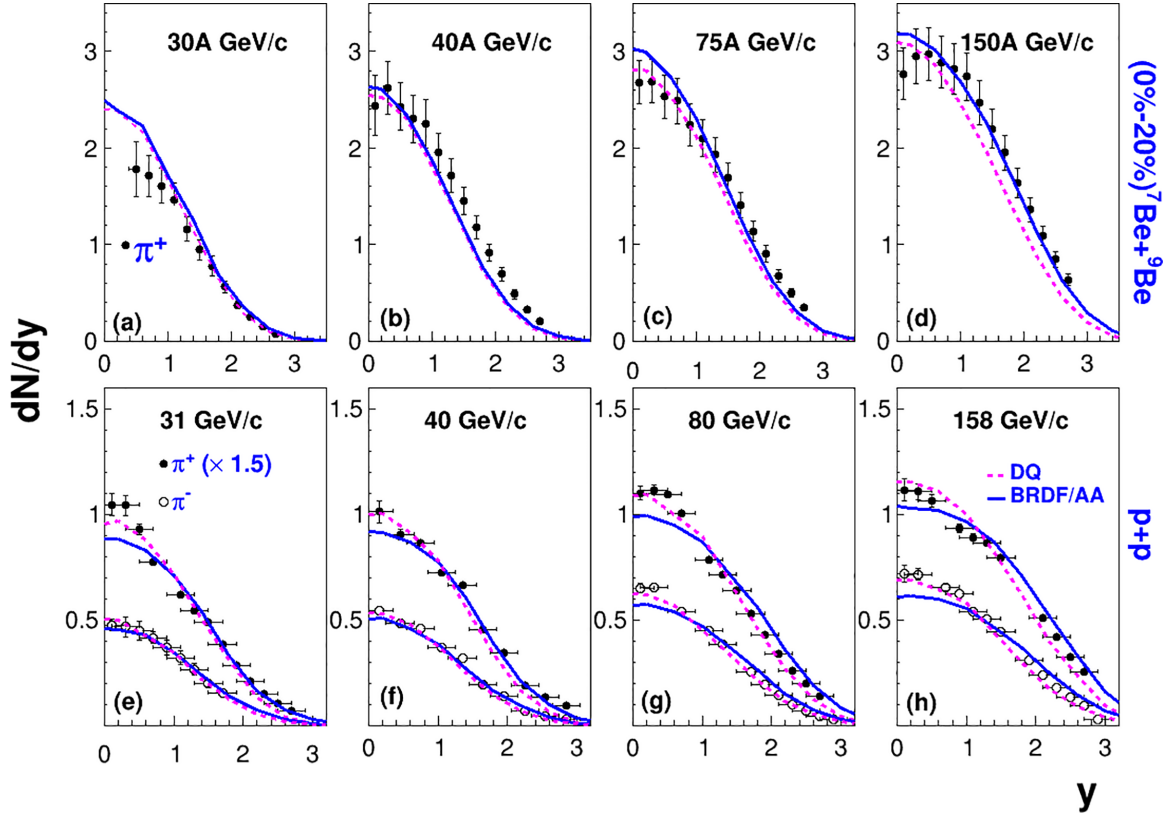
FIG. 9. The rapidity distributions of charged pions in inelastic pp collisions (lower panels) and 20% central Be + Be collisions (upper panels) at different SPS energies. The solid and small-dashed lines represent HIJING/AP results with the BRDF and diquark models, respectively. The closed points depict experimental data from NA61/SHINE measurements [1,2].

Figures 9 and 10 compare the results obtained from HIJING/diquark and HIJING/BRDF models with the measured rapidity distributions of charged pions and charged kaons generated by inelastic pp-collisions at various SPS energies. In both models, the dominant process that governs meson production is the LQ end of proton beam, where a quark and antiquark from neighboring breakups can combine to form a meson if the mass is appropriate. In the case of HIJING/BRDF, it is also possible to have a $BM\bar{B}$ configuration from both the LQ and LD ends of proton beam. To ensure a fair comparison between the models, the value of the strangeness suppression parameter (γ_s) is kept the same.

As shown in the lower panels of Figs. 9 and 10, the charged pion spectra of HIJING/diquark calculations (short-dashed lines) in inelastic pp collisions reproduce both the midrapidity yield and shape. However, the calculations overestimate the kaon yield at midrapidity. In contrast, the HIJING calculations with BRDF provide a better description of the kaon yield but underestimate the π^+ yield at midrapidity. Therefore, compared to the diquark model, the HIJING/BRDF calculations lead to greater suppression of mesons at midrapidity. This implies that the the $BM\bar{B}$ channel in the AP model is responsible for the reduction of mesons at midrapidity.

The upper panels of Figs. 9 and 10 present the results for charged pions and kaons in 20% central Be + Be collisions at SPS energies and compare them with the experimental

data from NA61/SHINE [2]. The figures indicate that the HIJING/diquark model nicely reproduces the π^+ rapidity spectra, except at the highest SPS energy. However, for the kaon yield, the model overestimates (underestimates) the K^+ yield at lower (higher) SPS energies. On the other hand, it is observed that the calculations with BRDF provide a better description of $\pi^\pm$ and $K^\pm$ rapidity spectra for the entire SPS energy range. Nevertheless, at forward rapidity ($y > 1$), both calculations underestimate the data for K^+ dN/dy at 75A GeV/c. This discrepancy could be related to the positive kaon enhancement reported in Ref. [25], for example, $p + p \rightarrow p + K^+ + \Lambda$, which is a production channel forbidden for K^-. It is noteworthy that the new thermal string fragmentation model [26] of PYTHIA 8.303 [27] model, which includes an exponential hadronic mass ($m_{\perp \text{had}}$) suppression, also cannot describe K^+ dN/dy better at the same beam momentum [28]. Therefore, further analysis is required to draw a definitive conclusion.

It should be noted here that the diquark model is inadequate in reproducing the positive pion and kaon rapidity distributions at the highest SPS energy for the "multiple" Be + Be collisions, as shown in Figs. 9(d) and 10(d). This model's failure occurs in the forward rapidity region ($y > 1$), despite its ability to accurately tune the corresponding π^+ and K^+ rapidity spectra in pp collisions to the measured pp data. This disparity may be linked to the high diffractive proton peak projected by the diquark model at high rapidity in Be + Be
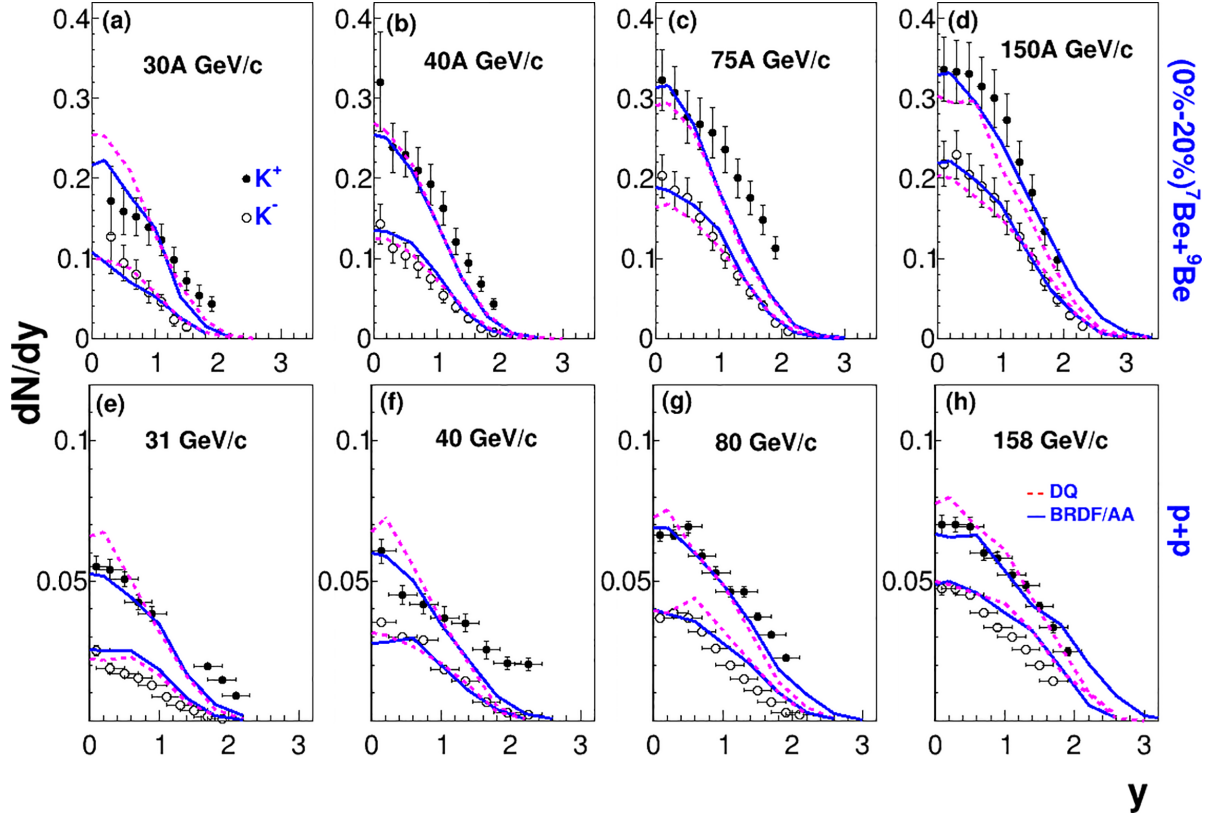
FIG. 10. Same as Fig. 9 but for charged kaons.

collisions [as shown in Fig. 8(d)], which is in sharp contrast to both the BRDF calculations and the experimental results.

The study of pp single-particle inclusive transverse (p_T) spectra is crucial for comprehending the dynamics of Be-Be collisions, given that different particles exhibit distinct systematic behaviors, as evident from Figs. 7–10. In the Lund string model's diquark and BRDF mechanisms, it is postulated that a string fragments into quark-antiquark ($q - \bar{q}$) pairs with a Gaussian distribution in transverse momentum. Moreover, the production of strange $q - \bar{q}$ pairs is suppressed by a factor of 0.22 in comparison to light ones. The hadrons are then produced from these quarks and antiquarks, with their production probability proportional to $\exp(-\pi m^2_\perp q/k)$. Here, $2m_{\perp q'} = 2\sqrt{m^2_{q'} + p^2_{q_\perp}}$ represents the transverse mass of the quark-antiquark pair, where $p_{q\perp}$ is the transverse momentum kick received by q and $\bar{q}$, with $p^2_{q\perp} = k/\pi = \sigma^2_{qq}$. The transverse momentum of a hadron, denoted by $\langle p_{T\text{had}} \rangle$, arises from the vector sum of its q and $\bar{q}$ kicks, giving $\langle p^2_{T\text{had}} \rangle = 2\sigma_{qq}$. Thus, in both mechanisms, the transverse momentum of hadrons is primarily governed by the diquark kick, which has a width of $\sigma_{qq} = 0.36$ GeV/c.

The inclusive p_T spectra of p, π^+, and K^+ in the HIJING model for central Be + Be collisions at midrapidity ($0 < y < 0.2$) are presented in Figs. 11 and 12. Both the diquark (short-dashed lines) and BRDF (solid lines) mechanisms are considered, with the same parameter values for the diquark p_T kick and longitudinal fragmentation parameters (a and b). The results show that the BRDF calculations provide a
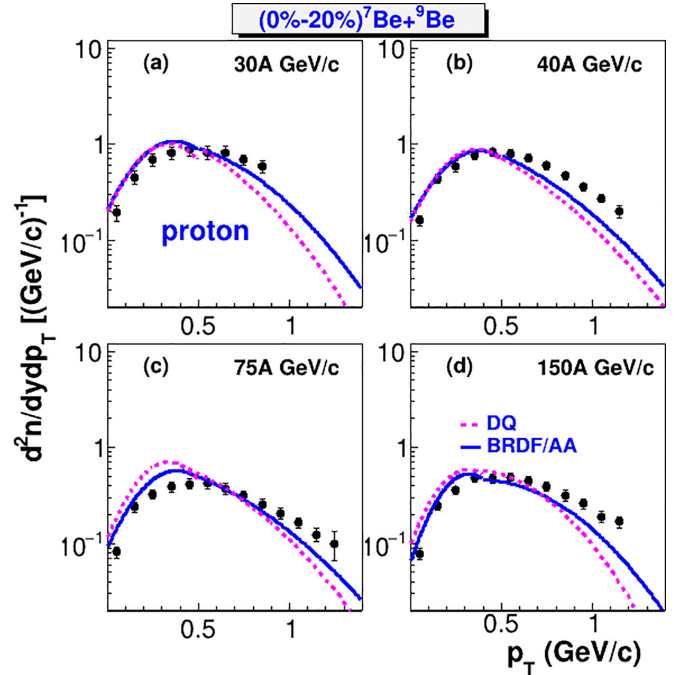

FIG. 11. The transverse momentum spectra of protons at midrapidity ($0 < y < 0.2$) in 20% central Be + Be collisions at SPS energies. The solid and small-dashed lines represent HIJING results with the BRDF and diquark models, respectively. The closed points depict experimental data from NA61/SHINE measurements [2].
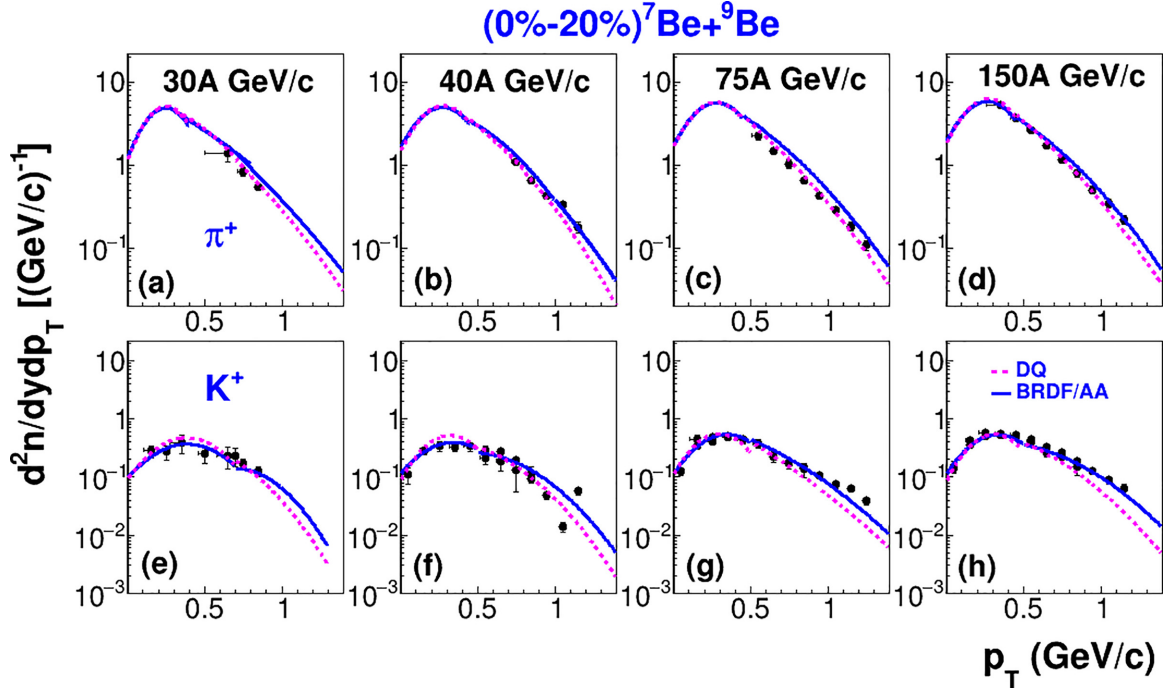
FIG. 12. Same as in Fig. 10, but for π^+ (upper panels) and K^+ (lower panels).

better fit to the data for the identified particles over the entire p_T range. However, the HIJING/diquark calculations exhibit significant deviations in the proton p_T distributions and are noticeably suppressed at high $p_T > 0.5$ GeV/c. Moreover, the BRDF effects enhance the production of heavier particles such as protons and K mesons more than the corresponding pion spectra. This observation may suggest that the identified particle spectra are sensitive to the popcorn baryon production mechanisms.

It is worth mentioning that the identified hadron spectra in central Be-Be collisions at CERN SPS energies were also explored using the new thermal model of PYTHIA8, as reported in Ref. [28]. In contrast to the Gaussian hadron-mass-independent tunneling formulas presented in Eq. (1), the thermal model utilizes an exponential hadronic mass suppression [26] during string breakup. The thermal model demonstrates similar trends as HIJING with BRDF for the entire range of SPS energies. Notably, the results in Ref. [28] show that the thermal model calculations reproduce the charged pions and kaons rapidities and p_T spectra quite well for the entire SPS energy range. Regarding protons, the thermal model reproduces the measured dN/dy satisfactorily, while underestimating proton p_T spectra in midrapidity ($0 < y < 0.2$) for $\sqrt{s_{NN}} \geqslant 30A$ GeV/c, due to medium effects. Indeed, it has been demonstrated that the incorporation of close packing of strings in the thermal model enhances p_T for all heavy particles, especially protons, whose p_T spectrum follows the experimental data remarkably well above 0.5 GeV/c.

It is important to highlight that baryon production within the HIJING model has always presented challenges when compared to experimental data. In our work, the issue has been addressed by incorporating the beam remnant diquark fragmentation (BRDF/AA) mechanism into HIJING. However, it

is worth noting that several other attempts have been made to tackle this problem, including the implementation of the gluon-baryon junction model [29–31]. This alternative approach suggests that baryon number traces in high-energy processes may reside in nonperturbative configurations of gluon fields, rather than in diquark-quark ($qq - q$) hadronic strings. In Refs. [30,31], a variant of the baryon junction mechanism, known as HIJING/B model, is implemented in HIJING. This model resolves the baryon around the "Y" junction through $q\bar{q}$ production, and the resulting three jet beams are fragmented as a $q - \bar{q}$ string. For reactions without junction exchange, standard $qq - q$ strings are used. The junction exchange is only allowed if the invariant mass of the excited "Y" configuration exceeds $m \geqslant 5$ GeV to ensure sufficient phase space for decay [30]. Once the junction has been exchanged, it remains stopped in subsequent soft interactions. The transverse momentum ($\vec{p}_T$) of the junction baryon is obtained by summing the $\vec{p}_T$ of the three sea quarks. The net proton (proton minus antiproton) and net hyperon (hyperon minus antihyperon) rapidity spectra predicted by HIJING and HIJING/B have been compared with $p + S$ data at $200A$ GeV/c and central Pb + Pb data at $158A$ GeV/c [30]. Reference [30] demonstrated that while HIJING significantly underpredicts both the observed stopping and hyperon production, the junction physics incorporated in HIJING/B sufficiently enhances both baryon stopping and hyperon production at midrapidity. However, as depicted in Fig. 1(d) of Ref. [30], this gluonic mechanism can only partially account for the observed hyperon enhancement in heavy Pb + Pb collisions. It should be noted that the predictions of the HIJING/B model at low SPS energies have not been published, and therefore, the gluon-baryon junction model warrants re-examination at such low SPS energies.

IV. SUMMARY AND CONCLUSIONS

This study examines the impact of popcorn baryon production mechanisms on the behavior of proton, $\pi^\pm$, and $K^\pm$ particles in 20% central Be + Be collisions at SPS beam momenta ranging from $30A$ to $150A$ GeV/c. To achieve this, HIJING was utilized, incorporating the advanced popcorn (AP) mechanism of baryon production from PYTHIA6.4. Two scenarios were considered: The diquark model and the AP model.

The AP mechanism allows for the implementation of beam remnant diquark fragmentation (BRDF), which results when a quark is expelled from a proton beam. The AP model offers two possible channels for baryon production from BRDF: The baryon-antibaryon ($B\bar{B}$) configuration, and configurations such as $BM\bar{B}$ and $BMM\bar{B}$, among others. In the diquark model, a $B\bar{B}$ is always produced from the diquark-antidiquark ($qq - \bar{q}\bar{q}$) pair production between the original ($q_0 - \bar{q}_0$) jet pair. The HIJING predictions were compared with each other and the measured identified particles at various SPS energies, utilizing the diquark and AP mechanisms and the parameter set from Table I. Based on the model calculations, the following conclusions can be drawn:

(1) The utilization of the diquark model is better suited for explaining the proton density at midrapidity compared to the default AP approach, which relied on the production of multiple $q - \bar{q}$ pairs for baryon production. However, the calculations using the diquark model result in an overestimation of the diffraction peak height as the energy of the beam increases.

(2) The default AP model predicts an unusual arrangement of peaks and dips in proton spectra detected at mid-rapidity. However, the incorporation of BRDF effects into HIJING/AP eliminates this anomalous pattern entirely.

(3) Incorporating BRDF effects provides an accurate depiction of proton behavior at mid-rapidity throughout the SPS energy range. Moreover, the diffractive peaks of protons at the highest SPS energy are adequately explained.

(4) The π^+ rapidity spectra are well reproduced by the HIJING/diquark model, except for the highest SPS energy. However, the model tends to overestimate (underestimate) the K^+ yield at lower (higher) SPS energies.

(5) Throughout the entire range of SPS energy, the $\pi^\pm$ and $K^\pm$ rapidity spectra are better described by HIJING calculations using BRDF.

(6) The BRDF calculations offer a better fit to the identified particle data across the entire p_T range. On the other hand, the HIJING/diquark calculations exhibit significant deviations in the proton and K^+ p_T distributions and are noticeably suppressed at high p_T (>0.5 GeV/c).

The new physics ingredient implemented in HIJING/AP focuses on treating baryon production mechanisms from both the leading quark and leading diquark endpoints of the proton beam. This implementation significantly improves the full-event Monte Carlo description of 20% central Be + Be collisions, especially at lower CERN SPS energies. Compared to the default popcorn baryon production mechanism implemented in PYTHIA event generator codes, the BRDF effects implemented in HIJING/AP can account for the proton stopping observables in central Be + Be collisions, while still producing $\pi^\pm$ and $K^\pm$ dN/dy and p_T spectra at midrapidity for the whole range of SPS energies. Therefore, the BRDF effect in HIJING/AP plays a noteworthy role in proton stopping in AA collisions at CERN SPS energies.

[1] A. Aduszkiewicz *et al.* (NA61/SHINE Collaboration), Eur. Phys. J. C **77**, 671 (2017).

[2] A. Acharya *et al.* (NA61/SHINE Collaboration), Eur. Phys. J. C **81**, 73 (2021).

[3] X.-N. Wang and M. Gyulassy, Phys. Rev. D **44**, 3501 (1991).

[4] Z. W. Lin and C. M. Ko, Phys. Rev. C **65**, 034904 (2002).

[5] S. Bass *et al.*, Prog. Part. Nucl. Phys. **41**, 255 (1998).

[6] B. Andersson, G. Gustafson, and B. Nilsson-Almqvist, Nucl. Phys. B **281**, 289 (1987).

[7] B. Nilsson-Almqvist and E. Stenlund, Comput. Phys. Commun. **43**, 387 (1987).

[8] T. Sjöstrand, Comput. Phys. Commun. **82**, 74 (1994).

[9] B. Andersson, G. Gustafson, and T. Sjöstrand, Nucl. Phys. B **197**, 45 (1982).

[10] B. Andersson, G. Gustafson, and T. Sjöstrand, Phys. Scr. **32**, 574 (1985).

[11] P. Edén and G. Gustafson, Z. Phys. C **75**, 41 (1997).

[12] K. Abdel-Waged and N. Felemban, Eur. Phys. J. Plus **137**, 1053 (2022).

[13] W. Cassing and E. L. Bratkovskaya, Phys. Rev. C **78**, 034919 (2008).

[14] J. Weil *et al.*, Phys. Rev. C **94**, 054905 (2016).

[15] T. Sjöstrand, S. Mrenna, and P. Skands, J. High Energy Phys. 05 (2006) 026.

[16] K. Abdel-Waged and N. Felemban, J. Phys. G: Nucl. Part. Phys. **47**, 065104 (2020).

[17] K. Abdel-Waged and N. Felemban, Phys. Rev. C **102**, 054904 (2020).

[18] N. Felemban, Nucl. Phys. A **1003**, 122033 (2020).

[19] J. Ranft, Phys. Rev. D **37**, 1842 (1988).

[20] K. Werner, Z. Phys. C **42**, 85 (1989).

[21] H.-U. Bengtsson and T. Sjöstrand, Comput. Phys. Commun. **46**, 43 (1987).

[22] T. Sjöstrand and M. van Zijil, Phys. Rev. D **36**, 2019 (1987).

[23] J. Schwinger, Phys. Rev. **82**, 664 (1951).

[24] B. Andersson, G. Gustafson, and B. Söderberg, Z. Phys. C **20**, 317 (1983).

[25] I. G. Bearden *et al.* (BRAHMS Collaboration), Phys. Rev. Lett. **90**, 102301 (2003).

[26] N. Fischer and T. Sjöstrand, J. High Energy Phys. 01 (2017) 140.

[27] T. Sjöstrand *et al.*, Comput. Phys. Commun. **191**, 159 (2015).

[28] K. Abdel-Waged and N. Felemban, Phys. Rev. C **105**, 024909 (2022).

[29] D. Kharzeev, Phys. Lett. B **378**, 238 (1996).

[30] S. E. Vance, M. Gyulassy, and X.-N. Wang, Phys. Lett. B **443**, 45 (1998).

[31] S. E. Vance and M. Gyulassy, Phys. Rev. Lett. **83**, 1735 (1999).